Available online at www.sciencedirect.com
ScienceDirect
Trans. Nonferrous Met. Soc. China 26(2016) 966−973
Transactions of Nonferrous Metals Society of China
www.tnmsc.cn

Strain rate-dependent high temperature compressive deformation characteristics of ultrafine-grained pure aluminum produced by ECAP

Ying YAN[1], Yue QI[1], Li-jia CHEN[2], Xiao-wu LI[1,3]

1. Institute of Materials Physics and Chemistry, School of Materials Science and Engineering, Northeastern University, Shenyang 110819, China;
2. School of Materials Science and Engineering, Shenyang University of Technology, Shenyang 110870, China;
3. Key Laboratory for Anisotropy and Texture of Materials, Ministry of Education, Northeastern University, Shenyang 110819, China

Received 20 April 2015; accepted 6 January 2016

Abstract: To explore the effect of strain rate $\dot{\varepsilon}$ on the high temperature deformation characteristics of ultrafine-grained materials, the deformation and damage features as well as microstructures of ECAP-treated pure Al at different temperatures T and strain rates $\dot{\varepsilon}$ were systematically studied through compression tests and microscopic observations. The increase in $\dot{\varepsilon}$ eliminates strain softening at T≤473 K, and largely enhances the yield strength and flow stress at 473−573 K. The shear deformation dominates the plastic deformation of ECAP-treated Al. Many cracks along shear bands (SBs) are formed at T≥473 K and secondary SBs basically disappear at 1×10^{-3} s^{-1}; however, at 1×10^{-2} s^{-1}, cracks are only observed at temperature below 473 K, and secondary SBs become clearer at T≥473 K. The microstructures of ECAP-treated Al mainly consist of sub-grains (SGs). The increase in $\dot{\varepsilon}$ inhibits the SG growth, thus leading to the increases both in yield strength and flow stress at high temperatures.

Key words: equal channel angular pressing (ECAP); pure Al; strain rate; high temperature compression; deformation; damage; microstructure

1 Introduction

It is well known that the bulk fine-grained materials have higher strength coupled with better plasticity and toughness. To obtain fine-grained or ultrafine-grained (UFG) materials, many kinds of mechanical processing techniques have thus been introduced. The severe plastic deformation (SPD), especially equal channel angular pressing (ECAP) technique, is one of the most frequently used mechanical processing methods. ECAP is an effective method to enhance the strength of metallic alloys through grain refinement by introducing intensive plastic strain into materials after repetitive pressing [1−5]. However, the microstructures of fine-grained or UFG materials prepared by ECAP present some characteristics similar to those of cold-worked materials [6], because their microstructures are at most in a metastable state with limited thermal and mechanical stabilities. The structural instability is a critical problem for practical engineering applications of such materials. As loading is exerted to the materials with a metastable microstructure at high temperatures, even at room temperature, the microstructure can be easily changed by dynamic recovery or recrystallization, thus leading to the degeneration of their mechanical properties [7−11]. For example, in UFG copper, as the compressive deformation temperature is in the range from room temperature to 573 K, the coarsening of grains occurred, and the coarsening behavior was related to strain rate, i.e., with raising strain rate, the localization phenomenon of grain coarsening becomes more remarkable [10]. The deterioration of mechanical properties of UFG materials largely restricts their uses in practical engineering under the comprehensive action of applied loading and temperature. Therefore, it is of practical significance to find some ways to improve the mechanical properties of UFG materials at high temperature.

Some researchers have reported that the UFG materials have an enhanced strain rate sensitivity of the

Foundation item: Projects (51231002, 51271054, 51571058, 50671023) supported by the National Natural Science Foundation of China
Corresponding author: Xiao-wu LI; Tel: +86-24-83678479; Fax: +86-24-83683674; E-mail: xwli@mail.neu.edu.cn
DOI: 10.1016/S1003-6326(16)64193-6

mechanical behavior compared with conventional-grained counterparts [11−19], and the sensitivity is strongly dependent upon the deformation temperature [11,12,16−19]. But these investigations mainly focus on the effects of temperature and strain rate on the mechanical behavior of UFG or nanocrystalline materials, while the variations in the deformation and damage features along with microstructures with the deformation temperature and strain rate are rarely considered [10−12]. Therefore, in the present work, pure Al processed by ECAP was chosen as the experimental material, and the effects of temperature and strain rate on the deformation and damage features as well as the corresponding microstructures were systematically investigated. The aim is to provide reference data for the potential application of UFG materials in engineering.

2 Experimental

Pure aluminum billet with 99.99% purity was used in the present study. A rod with 10 mm in diameter and 55 mm in length was cut from the original billet, and then processed by ECAP with a 90° angle channel and via route Bc to four passes at room temperature. The tetragonal compressive specimens with cross-sectional dimensions of 4 mm × 4 mm and a height of 6 mm were cut from the middle part of ECAP-treated Al rod to remove microstructural heterogeneity produced by ECAP processing, and the height direction of specimens is parallel to the rod axis. Before compression, the specimens were polished electrolytically to obtain a strain-free and clean surface for microscopic observations. The uniaxial compressive tests with loading direction parallel to the height direction of specimens (or rod axis) were conducted to an engineering strain of 45% using a CMT 5105 (made in China) testing machine with initial strain rates of 1×10^{-3} s^{-1} and 1×10^{-2} s^{-1}, respectively, at deformation temperatures ranging from 298 to 573 K. After compression tests, the deformation features near the central parts on the lateral surfaces and the corresponding microstructures were examined carefully by using SSX−550 scanning electron microscope (SEM) and TECNAI G^2 20 transmission electron microscope (TEM), respectively.

3 Results

3.1 Compressive stress−strain response

Figure 1 displays the compressive true stress−strain curves of ECAP-treated Al at various deformation temperatures, respectively, at two strain rates of 1×10^{-3} s^{-1} and 1×10^{-2} s^{-1}. Apparently, at a low strain rate of 1×10^{-3} s^{-1} (Fig. 1(a)), ECAP-treated Al undergoes a continuous strain hardening process at 298 K and 373 K. With increasing deformation temperature, strain softening followed by a finally slight strain hardening occurs after an initially rapid strain hardening. As temperature is above 473 K, the material undergoes an initially rapid strain hardening stage, and then enters into successive strain softening. In contrast, at a high strain rate of 1×10^{-2} s^{-1} (Fig. 1(b)), successive strain hardening or softening is exhibited at $T\leq473$ K and $T>473$ K, respectively.

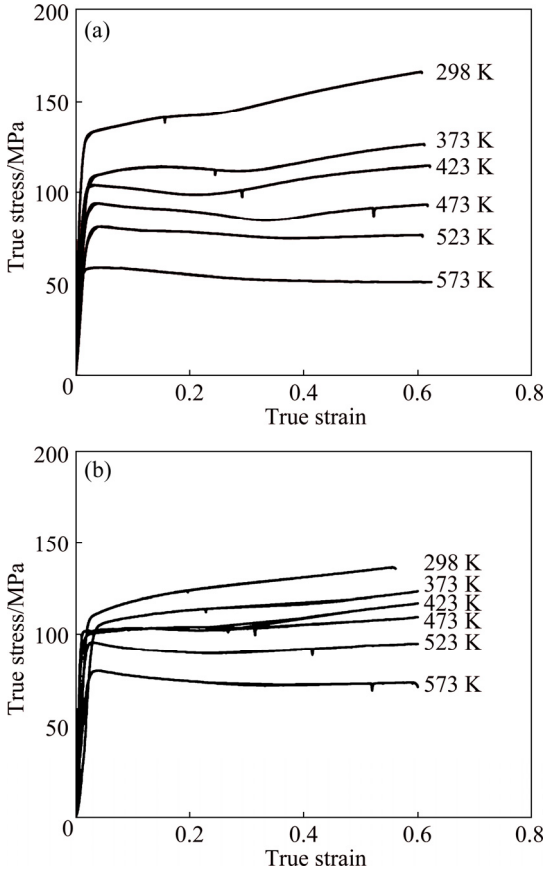

Fig. 1 True stress−strain curves of ECAP-treated Al compressed to engineering strain of 45% at different temperatures and two strain rates of 1×10^{-3} s^{-1} (a) and 1×10^{-2} s^{-1} (b)

To clearly reveal the influence of strain rate on the mechanical behavior of ECAP-treated Al at different temperatures, the compressive stress−strain curves at three typical deformation temperatures and the variation of yield strength (σ_{YS}) with T are demonstrated in Fig. 2. It can be found from Fig. 2(a) that an increase in strain rate leads to the disappearance of strain softening phenomenon at $T\leq473$ K and raises the flow stress and σ_{YS} at $T\geq473$ K. With raising T, the σ_{YS} monotonically decreases at 1×10^{-3} s^{-1}, whereas the σ_{YS} slowly decreases, and then increases at 473 K followed finally by a rapid decline at 1×10^{-2} s^{-1} (Fig. 2(b)).

3.2 Surface deformation and damage characteristics

The SEM images of surface deformation features

near the central parts on the lateral surfaces of ECAP-treated Al compressed at different temperatures and two strain rates are typically given in Figs. 3 and 4, respectively.

For all compressed samples, surface deformation characteristics are basically similar, namely, the large-scale shear bands (SBs) almost appear over the whole surface deformation regions. But there still exist some distinct differences at various deformation temperatures and the same strain rate. For example, with increasing T, the secondary SBs become more prominent at 1×10^{-3} s^{-1} (Figs. 3(a) and (b)). As T is 473 K, the amount of secondary SBs decreases and some cracks along SBs are formed (Fig. 3(c)). As T is raised up to as high as 573 K, the secondary SBs basically disappear and a number of cracks are observed (Fig. 3(d)). The similar results were also found in the UFG Cu, in which large-scale SBs cannot be formed at high temperature cyclic stressing [20]. However, in the case at 1×10^{-2} s^{-1}, the secondary SBs become more obvious with increasing T (Fig. 4), and only a small amount of micro-cracks are detected at 298 and 373 K, respectively (Figs. 4(a) and (b)).

In summary, the compressive plastic deformation of ECAP-treated Al is mainly governed by shear deformation in the form of SBs. With increasing T, the

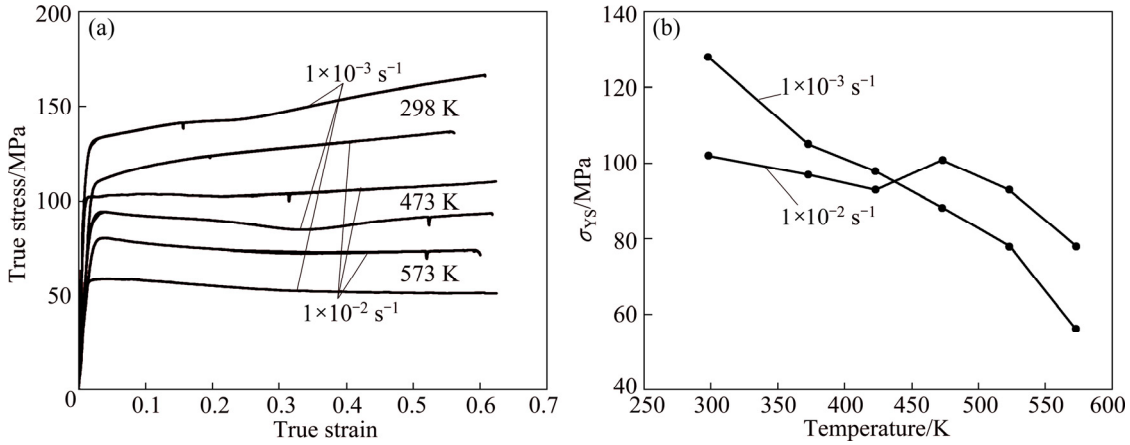

Fig. 2 Comparison of compressive true stress−strain curves of ECAP-treated Al at three typical deformation temperatures and two strain rates (a), and variation of σ_{YS} with deformation temperature at two strain rates (b)

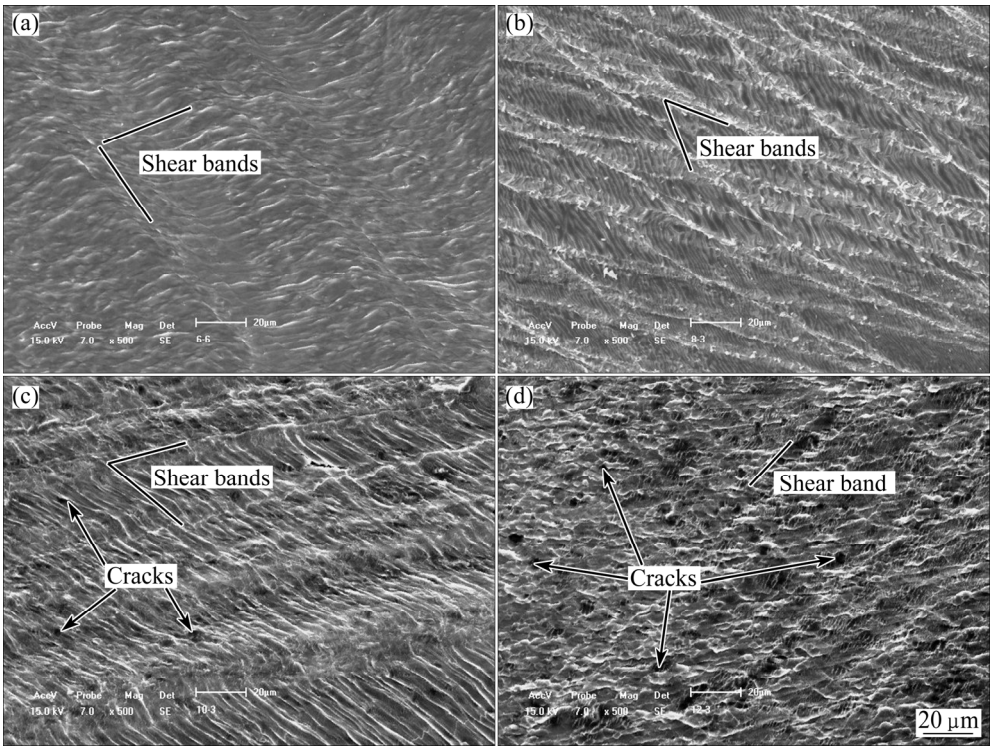

Fig. 3 SEM images of surface deformation features near central parts on lateral surfaces of ECAP-treated Al compressed at different temperatures and strain rate of 1×10^{-3} s^{-1}: (a) 298 K; (b) 373 K; (c) 473 K; (d) 573 K

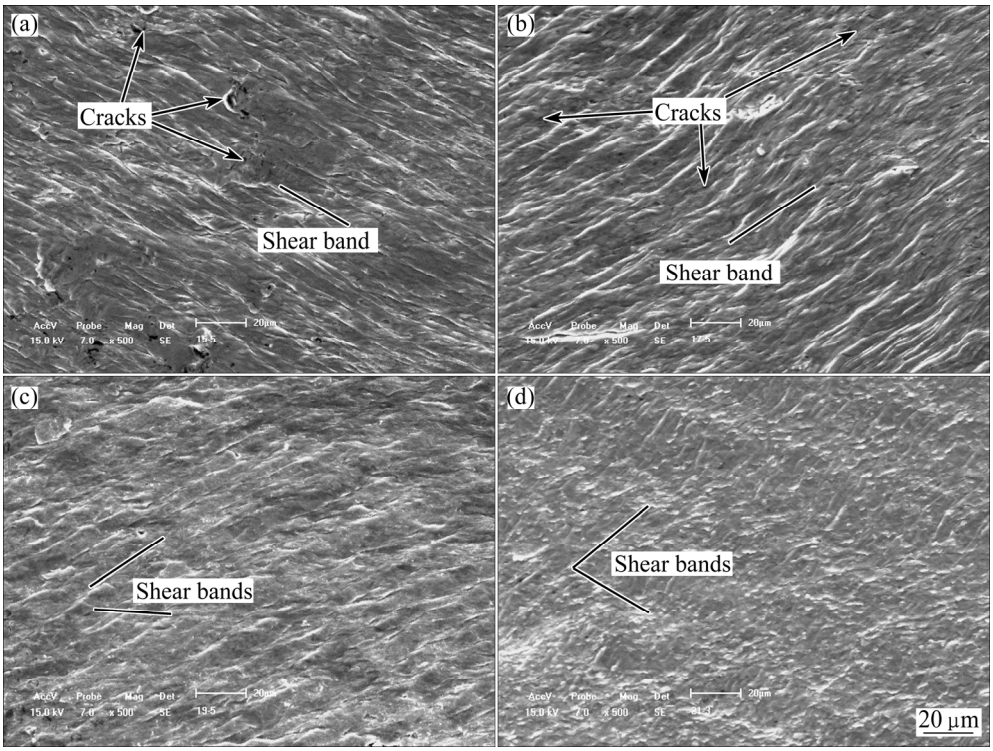

Fig. 4 SEM images of surface deformation features near central parts on lateral surfaces of ECAP-treated Al compressed at different temperatures and strain rate of 1×10^{-2} s^{-1}: (a) 298 K; (b) 373 K; (c) 473 K; (d) 573 K

secondary SBs in amount first increase and then decrease at 1×10^{-3} s^{-1}, even disappear at 573 K, and meanwhile, a lot of cracks are formed at $T\geq473$ K. Whereas at 1×10^{-2} s^{-1}, the secondary SBs become more obvious as T increases, and a small amount of micro-cracks are observed only at $T<473$ K.

3.3 Microstructures

Figure 5 displays the TEM images of the initial microstructures of as-ECAP-treated pure Al. The microstructure is primarily composed of sub-grains (SGs) with an average size of about 1 μm (Fig. 5(a)), and the dislocation density in some SGs is higher (Fig. 5(b)).

The TEM images of the ECAP-treated Al compressed to an engineering strain of 45% at different deformation temperatures and strain rates are given in Fig. 6.

The microstructures of ECAP-treated Al compressed at different deformation temperatures and strain rates are still composed of SGs, but their size and the density of dislocations in SGs vary with T and strain rate. For example, the average size of SGs at 1×10^{-3} s^{-1} is smaller than that at 1×10^{-2} s^{-1} and 298 K (Figs. 6(a) and (b)), which is attributed to the continuous occurrence of dynamic recovery at 1×10^{-3} s^{-1} induced by the combined effects of external loading and relatively high atom mobility at a low strain rate. As T is 473 K, the growth of SGs is observed, and their size distribution becomes non-uniform, especially at 1×10^{-3} s^{-1}, whereas the dislocation density in SGs is higher at 1×10^{-2} s^{-1} (Figs. 6(c) and (d)). As T is as high as 573 K, the growth of SGs becomes more remarkable, especially at 1×10^{-3} s^{-1}, and the dislocation density in SGs is still higher at 1×10^{-2} s^{-1} (Figs. 6(e) and (f)).

4 Discussion

The dislocations are difficult to generate from the GBs having a non-uniformly distorted dislocation structure for UFG metals and alloys processed by SPD [21,22]. The lack of sufficient dislocation activity leads to the operation of SBs as an alternative mechanism to sustain the applied strain [23], thus causing that the corresponding deformation and damage characteristics are manifested as the formation of a lot of SBs and cracks along SBs, as shown in Figs. 3 and 4. The similar phenomenon was also observed in UFG Al alloy [24], especially at higher strain rates.

To undertake the initial deformation, a certain number of SBs need to be initiated, and the initiated SBs can pass through the impediments, such as grain boundaries (GBs), sub-GBs or grain interiors. The above two processes determine the initial plastic deformation ability of materials. The change in flow stress during the compressive plastic deformation is primarily dependent upon the combined influences of the SB initiation and propagation abilities and the dynamic recovery or recrystallization degree. Pure Al has a higher stacking

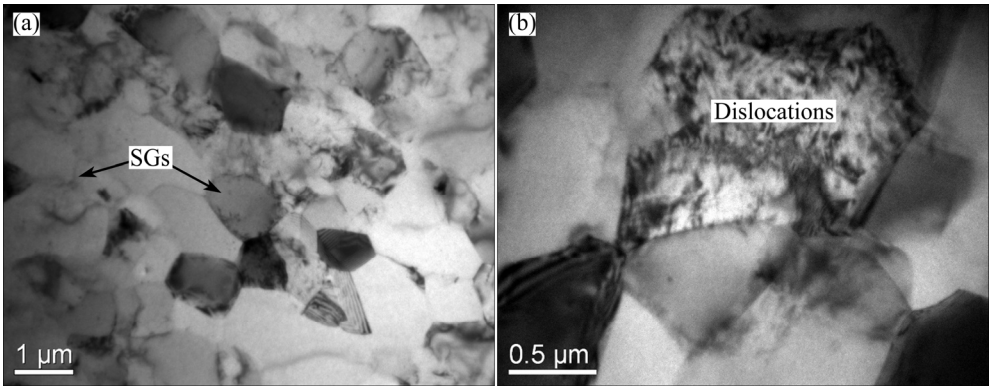

Fig. 5 TEM images showing initial microstructure of as-ECAP-treated pure Al

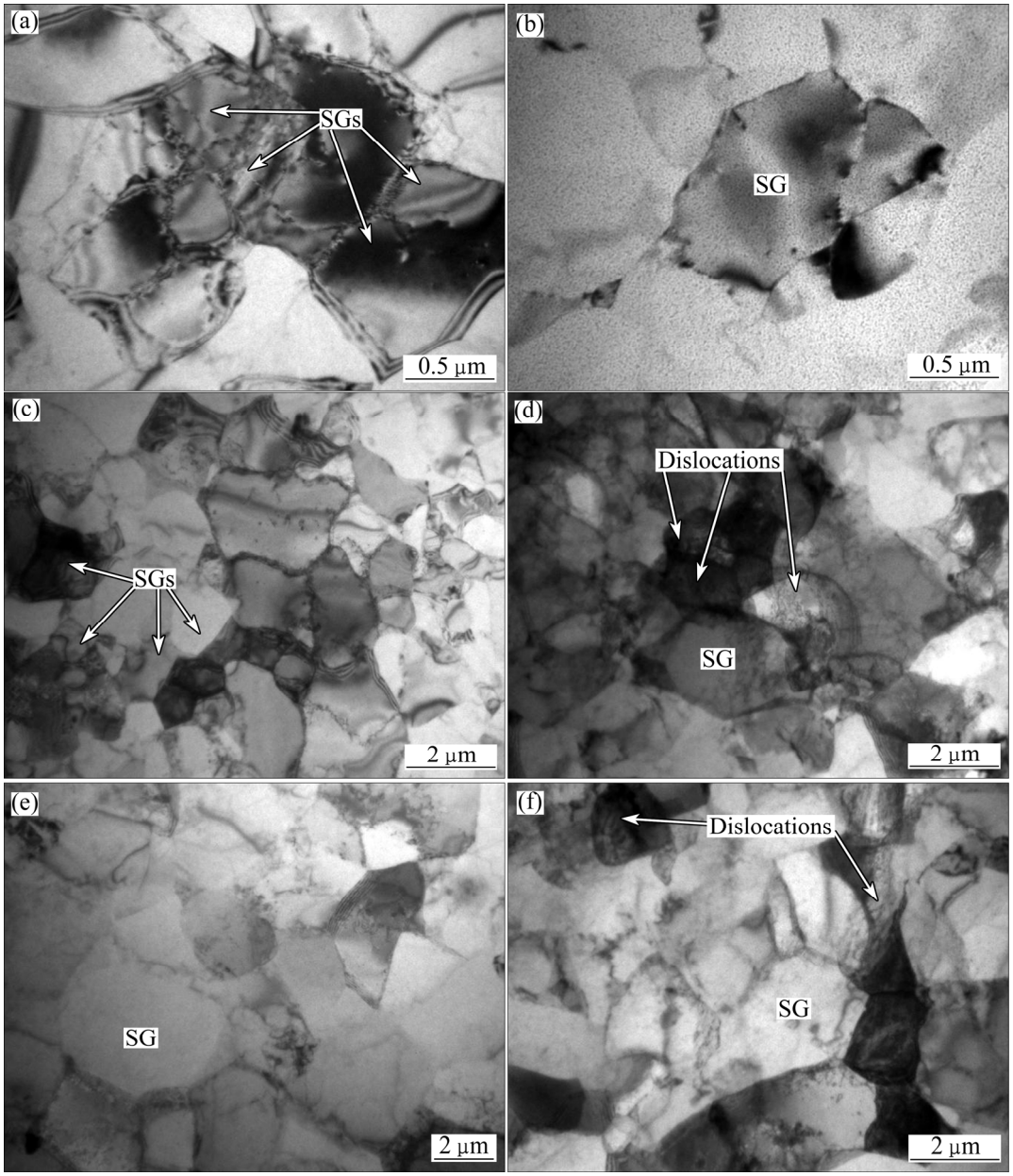

Fig. 6 TEM images of ECAP-treated Al compressed to engineering strain of 45% at different deformation temperatures and two strain rates: (a, c, e) 298, 473 and 573 K respectively at 1×10^{-3} s^{-1}; (b, d, f) 298, 473 and 573 K respectively at 1×10^{-2} s^{-1}

fault energy, and dynamic recovery is thus easier to occur during deformation due to rapid dislocation climb and cross slip, as shown in Figs. 5 and 6, namely, only SG structures are developed, even at T above the recrystallization temperature (≈(0.25−0.35)T_m, where T_m=933 K, the melting point of pure Al [25]); this is fully different from the case in UFG Cu with a medium stacking fault energy, for which dynamic recrystallization occurs at T above the recrystallization temperature [8,26,27].

The formation of SGs in as-ECAP-treated pure Al (Fig. 5) indicates that dynamic recovery occurred during ECAP processing, which will release a part of elastic strain energy introduced by ECAP, and the resistance to the formation and propagation of SBs is thus enhanced. However, the mobility of atoms is weak at a high strain rate, which will delay the release of residual elastic strain energy and the annihilation of mobile dislocations at GBs or sub-SGs, and thus promote the formation and propagation of SBs, resulting in the decrease of σ_{YS} at 1×10^{-2} s^{-1} and 298 K compared with the case at 1×10^{-3} s^{-1}. Here, the formation of SBs along single direction can bear the initial plastic deformation, but this also leads to the formation of some micro-cracks along SBs (Fig. 4(a)). With increasing T, the σ_{YS} continuously declines at two strain rates, but the difference in σ_{YS} becomes small due to the enhanced thermal activation of atoms along with enhanced dislocation mobility and easier GB motion. As T is close to or higher than the recrystallization temperature of pure Al, e.g., $T \geq 473$ K, static recovery first occurs, which has produced a detrimental influence for the SB formation and propagation; however, a low strain rate will lead to the growth of SGs, which not only promotes the dislocation slip [26], but also decreases the resistance of SB propagation, so the σ_{YS} continuously drops at 1×10^{-3} s^{-1}, and meanwhile, the SBs almost along one direction and a lot of micro-cracks are formed. However, for the case of 1×10^{-2} s^{-1}, slower atomic mobility inhibits the growth of SGs formed by static recovery, which will increase the resistance of SB propagation. In order to accommodate the initial deformation, the SBs along multiple directions need to be initiated, and the σ_{YS} is thus largely increased and much higher than that at 1×10^{-3} s^{-1} at the same T. Meanwhile, the initiation possibility of cracks along SBs declines due to the formation of SBs along multi-direction.

The flow stress during compression is characterized by strain softening followed with finally slight strain hardening at 1×10^{-3} s^{-1} as T is 423 K or 473 K. Although these two temperatures are below the recrystallization temperature of pure Al, dynamic recovery has taken place at two strain rates (Fig. 6). A low strain rate would lead to an earlier occurrence of dynamic recovery, and subsequently, the non-uniform growth of SGs takes place, thus leading to the first occurrence of strain softening. With continuous raising of strain amount, the SB formation becomes more difficult due to the occurrence of dynamic recovery and the growth of some SGs, as shown in Figs. 3(c) and (d), namely, secondary SBs become inconspicuous, which causes a finally slight strain hardening at 1×10^{-3} s^{-1}. However, at a high strain rate, dynamic recovery occurs later due to lower atomic mobility. In this case, the amount of accumulative elastic strain introduced by ECAP and subsequent compression deformation is higher, which promotes more intensive occurrence of dynamic recovery; meanwhile, the growth of SGs is not remarkable, because the compression test has finished before the occurrence of obvious SG coarsening. The fine-sized SGs formed by the rapid and intense dynamic recovery enhance the difficulty in SB formation and propagation, which offsets strain softening induced by dynamic recovery. Therefore, strain softening phenomenon disappears at 1×10^{-2} s^{-1}. As T is above 473 K, although it becomes more difficult for the formation and propagation of SBs, the notable growth of SGs along with the reinforced dislocation slip and GBs or sub-GBs motion result in the continuous decrease in flow stress at two strain rates. However, the flow stress is higher at 1×10^{-2} s^{-1}, which stems from the smaller size of SGs, higher density of dislocations in SGs, and the non-formation of cracks along SBs.

5 Conclusions

1) As the strain rate is 1×10^{-3} s^{-1}, ECAP-treated Al undergoes a strain softening stage followed by a finally slight strain hardening after an initially rapid strain hardening at deformation temperatures of 373 K and 473 K, whereas at 1×10^{-2} s^{-1}, strain softening phenomenon disappears. As T is above 473 K, continuous strain softening is exhibited at two strain rates. With raising T, the σ_{YS} monotonically decreases at 1×10^{-3} s^{-1}, whereas the σ_{YS} slowly decreases, and then increases at 473 K followed finally by a rapid decline at 1×10^{-2} s^{-1}. The increase in strain rate largely raises the σ_{YS} and flow stress at 473−573 K.

2) The compressive plastic deformation of ECAP-treated Al is mainly governed by shear deformation. The secondary SBs can be clearly observed with increasing T at 1×10^{-3} s^{-1}; however, as T≥473 K, the secondary SBs in amount decrease, even disappear, meanwhile, more cracks are formed. Whereas at 1×10^{-2} s^{-1}, the secondary SBs become more obvious

with increasing T, and micro-cracks are only observable at T below 473 K.

3) The microstructures of as-produced and uniaxially compressed ECAP Al samples are primarily composed of SGs. The increase in strain rate prohibits the coarsening of SGs, thus leading to a uniform size distribution of SGs.

References

[1] YANG Q, GHOSH A K. Deformation behavior of ultrafine-grain (UFG) AZ31B Mg at room temperature [J]. Acta Materialia, 2006, 54: 5159−5170.

[2] FANG D R, ZHANG Z F, WU S D, HUANG C X, ZHANG H, ZHAO N Q, LI J J. Effect of equal channel angular pressing on tensile properties and fracture modes of casting Al−Cu alloys [J]. Materials Science and Engineering A, 2006, 426: 305−313.

[3] CHEN Bin, LIN Dong-liang, JIN Li, ZENG Xiao-qin, LU Chen. Equal-channel angular pressing of magnesium alloy AZ91 and its effects on microstructure and mechanical properties [J]. Materials Science and Engineering A, 2008, 483−484: 113−116.

[4] EI-DANAF E A. Mechanical properties and microstructure evolution of 1050 aluminum severely deformed by ECAP to 16 passes [J]. Materials Science and Engineering A, 2008, 487: 189−200.

[5] CAVALIERE P. Fatigue properties and crack behavior of ultra-fine and nanocrystalline pure metals [J]. International Journal of Fatigue, 2009, 31: 1476−1489.

[6] MOLODOVA X, GOTTSTEIN G, WINNING M, HELLMIG R J. Thermal stability of ECAP processed pure copper [J]. Materials Science and Engineering A, 2007, 460−461: 204−213.

[7] LI X W, UMAKOSHI Y, WU S D, WANG Z G, ALEXANDROV I V, VALIEV R Z. Temperature effects on the fatigue behavior of ultrafine-grained copper produced by equal channel angular pressing [J]. Physica Status Solidi (a), 2004, 201: R119−122.

[8] YU Zhao-yuan, JIANG Qing-wei, LI Xiao-wu. Temperature-dependent deformation and damage behavior of ultrafine-grained copper under uniaxial compression [J]. Physica Status Solidi (a), 2008, 205: 2417−2421.

[9] LONG Feng-wu, JIANG Qing-wei, XIAO Lin, LI Xiao-wu. Compressive deformation behaviors of coarse- and ultrafine-grained pure titanium at different temperatures: A comparative study [J]. Materials Transactions, 2011, 52: 1617−1622.

[10] JIANG Qing-wei, LIU Yin, WANG Yao, CHAO Yue-sheng, LI Xiao-wu. Microstructural instability of ultrafine-grained copper under annealing and high-temperature deformation [J]. Acta Metallurgica Sinica, 2009, 45: 873−979. (in Chinese)

[11] LI Xiao-wu, JIANG Qing-wei, LIU Yin, WANG Yao. Effect of strain rate on the high-temperature compressive deformation behavior of ultrafine-grained copper [J]. International Journal of Modern Physics B, 2009, 23: 1758−1763.

[12] MAY J, HÖPPEL H W, GÖKEN M. Strain rate sensitivity of ultrafine-grained aluminium processed by severe plastic deformation [J]. Scripta Materialia, 2005, 53: 189−194.

[13] CONRAD H, JUNG K. On the strain rate sensitivity of the flow stress of ultrafine-grained Cu processed by equal channel angular extrusion (ECAE) [J]. Scripta Materialia, 2005, 53: 581−584.

[14] LI Y J, ZENG X H, BIUM W. Transition from strengthening to softening by grain boundaries in ultrafine-grained Cu [J]. Acta Materialia, 2004, 52: 5009−5018.

[15] DALLA TORRE F H, PERELOMA E V, DAVIES C H J. Strain rate sensitivity and apparent activation volume measurements on equal channel angular extruded Cu processed by one to twelve passes [J]. Scripta Materialia, 2004, 51: 367−371.

[16] FARROKH B, KHAN A S. Grain size, strain rate, and temperature dependence of flow stress in ultra-fine grained and nanocrystalline Cu and Al: Synthesis, experiment, and constitutive modeling [J]. International Journal of Plasticity, 2009, 25: 715−732.

[17] SUO Tao, LI Yu-long, ZHAO Feng, FAN Xue-ling, GUO Wei-guo. Compressive behavior and rate-controlling mechanisms of ultrafine grained copper over wide temperature and strain rate [J]. Mechanics of Materials, 2013, 61: 1−10.

[18] GRAY III G T, LOWE T C, CADY C M, VALIEV R Z, ALEKSANDROV I V. Influence of strain rate & temperature on the mechanical response of ultrafine-grained Cu, Ni, and Al−4Cu−0.5Zr [J]. Nanostructured Materials, 1997, 9: 477−480.

[19] TANG Zhong-bin, SUO Tao, ZHANG Bu-sheng, LI Yu-long, ZHAO Feng, FAN Xue-ling. Uniaxial compressive behavior of equal channel angular pressing Al at wide temperature and strain rate range [J]. Transactions of Nonferrous Metals Society of China, 2014, 24: 2447−2452.

[20] LI X W, WU S D, WU Y, YASUDA H Y, UMAKOSHI Y. Surface deformation features in ultrafine-grained copper cyclically stressed at different temperatures [J]. Materials Transactions, 2005, 46: 3077−3080.

[21] VALIEV R Z. Approach to nanostructured solids through the studies of submicron grained polycrystals [J]. Nanostructured Materials, 1995, 6: 73−82.

[22] VALIEV R Z. Structure and mechanical properties of ultrafine-grained metals [J]. Materials Science and Engineering A, 1997, 234−236: 59−66.

[23] MALEKJANI S, HODGSON P D, STANFORD N E, HILDITCH T B. The role of shear banding on the fatigue ductility of ultrafine-grained aluminium [J]. Scripta Materialia, 2013, 68: 269−272.

[24] SABIROV I, BARNETT M R, ESTRIN Y, HODGSON P D. The effect of strain rate on the deformation mechanisms and the strain rate sensitivity of an ultra-fine-grained Al alloy [J]. Scripta Materialia, 2009, 61: 181−184.

[25] CUI Zhong-qi. Metallurgy and heat treatment [M]. 5th ed. Beijing: Mechanical Industry Press, 2002. (in Chinese)

[26] JIANG Qing-wei, XIAO Lin, LI Xiao-wu. A comparison of temperature-dependent compressive deformation features of ultrafine-grained Ti and Cu produced by ECAP [J]. Materials Science Forum, 2011, 682: 41−45.

[27] BLUM W, LI Y J, DURST K. Stability of ultrafine-grained Cu to subgrain coarsening and recrystallization in annealing and deformation at elevated temperatures [J]. Acta Materialia, 2009, 57: 5207−5217.

等通道转角挤压超细晶纯铝高温压缩变形特点的应变速率依赖性

颜 莹[1]，齐 跃[1]，陈立佳[2]，李小武[1,3]

1. 东北大学 材料科学与工程学院 材料物理与化学研究所，沈阳 110819；
2. 沈阳工业大学 材料科学与工程学院，沈阳 110870；
3. 东北大学 材料各向异性与织构教育部重点实验室，沈阳 110819

摘 要：为了探索应变速率对超细晶材料高温变形特点的影响，通过压缩实验以及显微观察，系统研究在不同温度和应变速率下等通道转角挤压 Al 的变形和损伤特点以及显微微组织。结果表明：应变速率的提高消除了等通道转角挤压 Al 在变形温度 $T\leq 473$ K 时表现出的应变软化现象，并且大大提高了变形温度在 473~573 K 范围的屈服强度和流变应力。等通道转角挤压 Al 的塑性变形主要由剪切变形控制。当应变速率为 1×10^{-3} s^{-1} 时，变形温度 $T\geq 473$ K 时可观察到沿剪切带形成了大量裂纹，并且二次剪切带基本消失。而当应变速率为 1×10^{-2} s^{-1} 时，只有在变形温度低于 473 K 时才能观察到沿剪切带形成的裂纹，并且当压缩温度 $T\geq 473$ K 时，二次剪切带变得更加清晰。等通道转角挤压 Al 的显微组织主要由亚晶组成，应变速率的提高抑制了亚晶的长大，从而导致高温屈服强度和流变应力的提高。

关键词：等通道转角挤压；纯铝；应变速率；高温压缩；变形；损伤；显微组织

(Edited by Xiang-qun LI)